

Invited Paper

Large Device Fabrication of Electrochromic Smart Windows with Fe(II)-Based Metallosupramolecular Polymer

Shifa Sarkar[†,††], Kazuhiko Sakata[†], Yukio Fujii[†] and Masayoshi Higuchi[†,††*]

Abstract Large (200 × 200 mm) electrochromic (EC) devices were fabricated using Fe(II)-based metallosupramolecular polymer (MSP) as the EC material, nickel hexacyanoferrate (NiHCF) as the counter electrode material, and $LiClO_4$ solution as the electrolyte. The fabricated EC devices were installed in a south-facing window of a high-rise building in the Ibaraki Prefectural Government Office. After about one year of practical use, a reversible color change between purple and colorless was confirmed on the EC smart window, suggesting the high durability of the EC device. The fading of the Ibaraki device in the colored state was confirmed by a higher transmittance (12%) than the standard reference (STD) device (3%). The STD device exhibited 57% optical contrast at 580 nm between +1.5 and 0 V, while the Ibaraki device maintained 66% between +3.0 and 0 V.

Keywords: metallosupramolecular polymer, electrochromic, large-size, smart window.

1. Introduction

The increasing global demand for energy-efficient technologies in the building sector has driven significant advancements in smart window systems that can dynamically regulate light and heat transmission.[1-3] Buildings are responsible for a considerable portion of global energy consumption, particularly in heating, ventilation, air conditioning, and lighting.[4] Traditional static glazing materials, while effective in providing insulation, do not offer adaptive control over light and thermal transmittance, leading to excessive energy consumption in response to seasonal and daily fluctuations in temperature and sunlight exposure.[5] Electrochromic (EC) smart windows have emerged as a transformative solution, allowing dynamic control over optical properties via an externally applied low voltage.[6, 7] These windows transition between transparent and colored states, thereby optimizing indoor lighting conditions and reducing reliance on artificial climate control, ultimately leading to energy conservation and enhanced occupant comfort.[8, 9]

To date, a variety of EC materials have been explored, ranging from inorganic transition metal oxides such as tungsten trioxide and nickel oxide, to organic-based systems such as viologens, and conductive polymers like polyaniline and poly(3, 4-ethylenedioxythiophene).[10, 11] While these materials have demonstrated significant advancements in terms of color variation, switching efficiency, and durability, each has inherent limitations.[12] Metal oxides often require high-temperature processing and may exhibit sluggish switching times, limiting their practical application in large-area coatings. Organic viologens and conductive polymers, while offering greater tunability in coloration, can suffer from long-term stability issues due to degradation under prolonged redox cycling.[13] Additionally, the cost and scalability of these materials remain critical concerns for real-world applications.[14] Consequently, there is a continued search for alternative EC materials that combine ease of fabrication, structural robustness, fast response times, and stable performance over extended usage.[15, 16]

Metallosupramolecular polymers (MSPs) have emerged as an especially promising class of EC materials.[17, 18] Formed through coordination bonds between metal centers and organic ligands, these polymers can be tailored to exhibit specific redox

Received June 18, 2025; Revised September 10, 2025; Accepted September 17, 2025

† National Institute for Materials Science (NIMS)
(Ibaraki, Japan)
†† Graduate School of Information Science and Technology, The University of Osaka
(Osaka, Japan)
*Corresponding author, HIGUCHI.Masayoshi@nims.go.jp

**This paper includes videos. Note that the videos are not viewable from this PDF file. The videos are available as separate files on the website that hosts this PDF file.

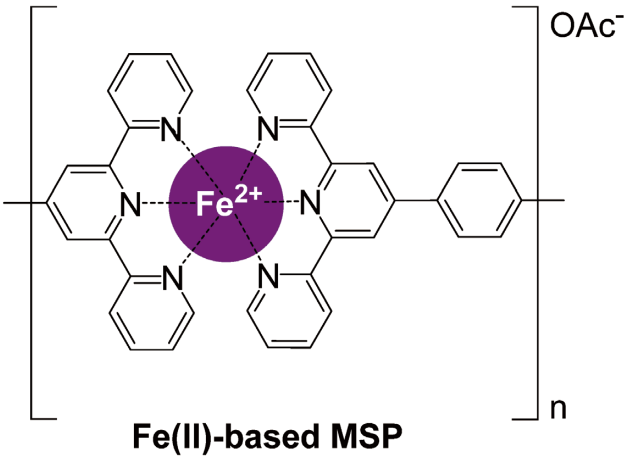

Fig. 1 The chemical structure of Fe(II)-based MSP.

potentials, coloration properties, and mechanical characteristics.[19-21] Among the variety of possible metal-ligand frameworks, Fe(II)-based MSPs (Fig. 1) stand out due to their cost-effectiveness, fast redox kinetics, high structural stability over multiple switching cycles, and pronounced color changes associated with the Fe(II)/Fe(III) transitions.[22, 23] Beyond their favorable EC properties, Fe(II)-based MSPs benefit from iron's relative abundance and low toxicity, making them suitable for large-scale commercial applications.[24, 25]

In this work, we describe the fabrication and real-world testing of an EC smart window based on Fe(II)-based MSP (polyFeL1) and performance evaluation using an image-based analytical technique. Through this work, we contribute to the growing body of evidence indicating that polyFeL1 can offer both the functionality and durability necessary for sustainable architectural applications. By thoroughly investigating the scientific principles guiding material design, such as bonding interactions, structural stability, and environmental resilience—we also assess the practicality of large-scale implementation in real-world building projects.

2. Experiment

2.1 Chemicals and instruments

All materials were of reagent grade and employed as supplied, without any additional purification. Indium tin oxide (ITO)-coated glass substrates (resistivity of 5 Ω/sq) were obtained from Sigma-Aldrich Co. LLC. Propylene carbonate (PC), and methanol (MeOH) were purchased from Wako Pure Chemical Industries, Ltd. Nickel hexacyanoferrate (NiHCF) and lithium perchlorate ($LiClO_4$) were supplied by Kanto Chemical Co., Inc. The polyFeL1 was obtained from Tokyo Chemical Industry (TCI) Co., Ltd.

An automated spray coating machine manufactured by Apeiros API Corporation (Tokyo), was used to prepare polyFeL1 and counter-material films.

2.2 Preparation of polymer solution

PolyFeL1 (3.5 mg/mL) was first dissolved in MeOH, and the resulting mixture was stirred for one hour. Before preparing the polymer film, the solution was passed through a 0.45 μm PVDF syringe filter to remove any insoluble residues.

2.3 Preparation of electrolyte

In a typical procedure, $LiClO_4$ was dissolved in the plasticizer (PC) under vigorous stirring, maintaining a $LiClO_4$/PC weight ratio of 1/113. Stirring continued for 30 minutes, yielding a colorless, transparent liquid electrolyte.

2.4 Dimensional measurement of ITO glass substrates

Measurements of 200 × 200 mm bare ITO glass substrates (Table 1) were performed to evaluate their suitability for conductive electrode deposition and subsequent lamination steps of the base materials. The measured average lengths (200 mm) and thickness (0.71

Table 1 Dimensional measurement of 200 × 200 mm ITO glass substrates.

	L direction (mm)			T direction (mm)			Thickness (mm)				
ITO glass substrates	L1	L2	L3	T1	T2	T3	d1	d2	d3	d4	d5
No.1	200.04	199.98	200.02	199.99	200.01	200.01	0.71	0.71	0.71	0.71	0.71
No.2	200.00	199.99	199.98	200.00	199.99	200.02	0.71	0.71	0.71	0.71	0.71
No.3	200.01	200.01	199.98	200.00	200.00	200.03	0.71	0.71	0.71	0.71	0.71
Number of measurements	9			9			15				
Average value	200.00			200.01			0.71				
Standard deviation	0.020			0.013			0.000				
Maximum-minimum value	0.06			0.04			0.000				

mm) remained remarkably consistent, with standard deviations near 0.013 mm and a negligible maximum-minimum difference (0.06 mm in planar dimensions; 0.00 mm in thickness), emphasizing the superior dimensional stability of the raw substrates. These findings confirmed that the ITO glass substrates exhibited the dimensional accuracy, minimal thickness variation, and uniform electrode design needed for large-scale smart windows.

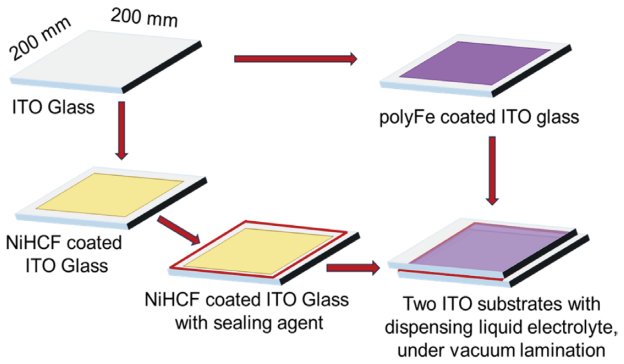

Scheme 1 Fabrication of large ECD with liquid electrolyte.

3. Result and Discussion

3.1 Device Fabrication

To fabricate the electrochromic device (ECD) (Scheme S1), indium tin oxide (ITO)-coated glass substrates (200 × 200 mm) were used as the base layer. Prior to assembly, the ITO substrates underwent thorough cleaning, they were first subjected to ultrasonic treatment in acetone for 15 minutes, then boiled in isopropyl alcohol for 5 minutes, and finally exposed to ultraviolet-ozone for 20 minutes to eliminate organic residues and any other potential contaminants.

The ITO substrate was placed on a hot plate maintained at 58-60 °C and secured at the corners with masking tape. The filtered iron polymer solution was then applied via spray-coating, producing a smooth and uniform film, used as the working electrode (WE). Approximately 120 mL of solution were required for a 200 × 200 mm substrate, with the coating process repeated 3 times to achieve the required film thickness. Similarly, the counter material film was prepared on the separate ITO glass substrate at 95 °C using a water solution of NiHCF, used as counter electrode (CE). To get the required film thickness, the coating process was repeated twice.

Once the electrodes were fully prepared, a sealing agent was precisely applied along the peripheral edges of the CE (NiHCF-coated substrate). This seal created a protective boundary to contain the electrolyte and prevent leakage. Following the application of the sealant, the WE substrate was carefully aligned and positioned over the CE. The two substrates were brought into contact under a vacuum-assisted lamination process, during which a precisely measured volume of transparent electrolyte solution was introduced into the cell gap. This step was crucial in removing trapped air, ensuring complete electrolyte infiltration, and promoting uniform contact between the active layers. Proper alignment was carefully maintained to prevent short circuits and ensure homogeneous spacing, which are critical for optimal device performance. Once the assembly was complete, the peripheral seal was cured using UV exposure, ensuring a strong, permanent enclosure of the electrolyte within the device (Scheme 1).

At this stage, the device was typically inspected for uniformity in layer thickness and sealing integrity. The resulting structure featured a well-defined active region, isolated from the environment.

3.2 Dimensional Analysis of Laminated ECDs

After fabrication of ECDs dimensional measurements were carried out by taking five laminated ECD samples (No.1 ECD to No.5 ECD), which demonstrate a consistent and reliable lamination process in both planar dimensions (L and T directions) and overall thicknesss (d), suitable for large area smart window applications. Each sample was measured at three points along the length (L1, L2, L3), three points along the width (T1, T2, T3), and five points for thickness (d1–d5) (Fig. 2) (resembling the dimensional measurement of ITO substrates). As summarized in Table 2, measurements along the L direction were approximately 204–205 mm, while those along the T direction were around 200 mm, with a maximum difference of 0.59 mm between the largest and smallest measured values. The thickness, measured at five points (d1–d5) on each

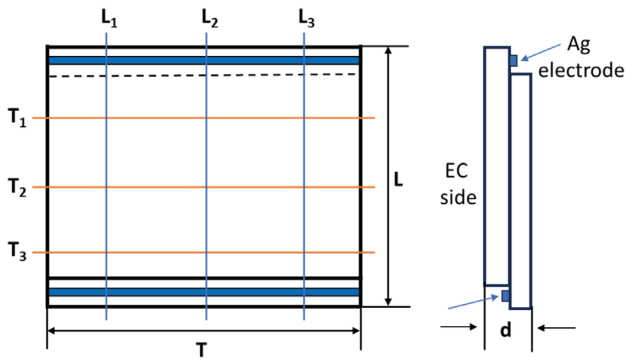

Fig. 2 Dimensional analysis of laminated ECDs.

Table 2 Dimensional measurement of laminated ECDs.

	L direction (mm)			T direction (mm)			Thickness (mm)				
Laminated product	L1	L2	L3	T1	T2	T3	d1	d2	d3	d4	d5
No.1 ECD	204.67	204.91	205.07	200.16	200.07	200.02	1.60	1.51	1.50	1.60	1.59
No.2 ECD	204.65	204.95	205.22	200.25	200.14	200.14	1.59	1.54	1.53	1.59	1.60
No.3 ECD	204.86	205.03	205.30	200.24	200.16	200.09	1.55	1.54	1.53	1.60	1.54
No.4 ECD	204.90	205.19	205.33	199.95	200.07	200.34	1.57	1.59	1.52	1.60	1.51
No.5 ECD	204.68	204.87	204.95	200.06	200.12	200.21	1.52	1.53	1.52	1.58	1.57
Number of measurements	15			15			25				
Average value	204.97			200.16			1.56				
Standard deviation	0.21			0.13			0.03				
Maximum-minimum value	0.68			0.59			0.10				

sample, ranges from about 1.50 to 1.60 mm, with a maximum variation of only 0.10 mm. The results revealed that the lamination process was well controlled, yielding uniform sheets within acceptable tolerances for ECD fabrication. In addition, in these EC samples (ECDs), a conductive silver (Ag) electrode was applied along the edges of each ITO-coated glass substrate. This silver layer served as the current collector, enhancing the electrical contact between the external power supply and the ITO electrode. Positioning the Ag electrode precisely at the edges minimized the potential drop across the device, thereby promoting uniform charge distribution over the EC film. The consistency demonstrated across multiple samples underscores the reproducibility and robustness of the lamination process. Ensuring dimensional uniformity was essential for smart window application, as uneven panel thickness or inconsistent planar dimensions can result in non-uniform electrical fields, leading to uneven coloration and inconsistent switching times.

3.3 Installation of EC smart window

During this project, a structured and precise installation process was successfully demonstrated for a large-scale EC smart window in a high-rise building in the Ibaraki Prefectural Government Office (Fig. 3). A custom-built wooden framework, measuring 2, 462 mm

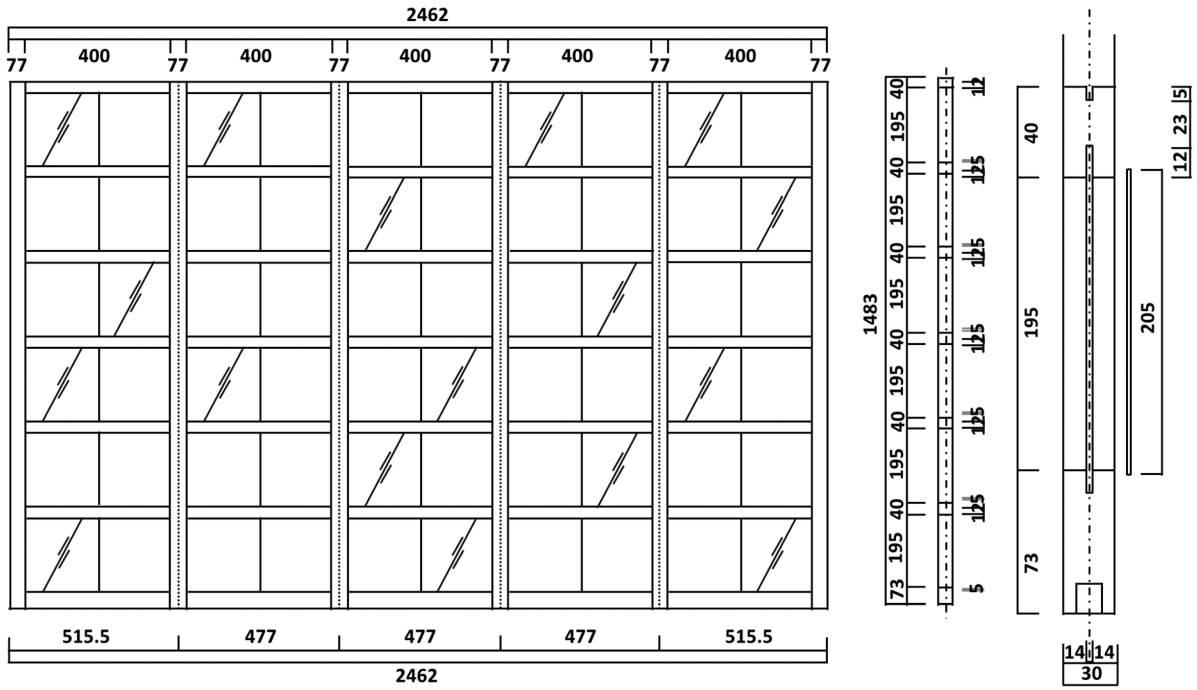

Fig. 3 Diagram of wooden framework for installation of EC smart window.

in width, 1, 483 mm in height, and 205 mm in depth, was meticulously designed and constructed to accommodate 60 ECDs, each measuring 200 × 200 mm. The framework was thoughtfully organized into a grid, consisting of inner columns 477 mm wide, outer columns 515.5 mm wide, and horizontal rails of 195 mm in height, separated by rails 40 mm thick. This precise configuration allowed each compartment to securely fit exactly two EC panels. Special attention was given to the precise measurement and consistent rebate depths to facilitate proper sealing for airtight and watertight insulation. Electrical wiring was methodically integrated through specifically designed wiring channels measuring 14 mm deep by 30 mm wide within the wooden frame, providing neat and concealed connections to the appropriate voltage supply. Upon applying voltage, uniform EC behavior was observed across all panels, confirming the effectiveness and accuracy of the installation and wiring processes. The successful implementation demonstrated that detailed measurement planning, coordinated carpentry efforts, and careful integration of electrical systems could reliably achieve large-scale EC smart window installations, providing consistent functionality, visual appeal, and energy efficiency.

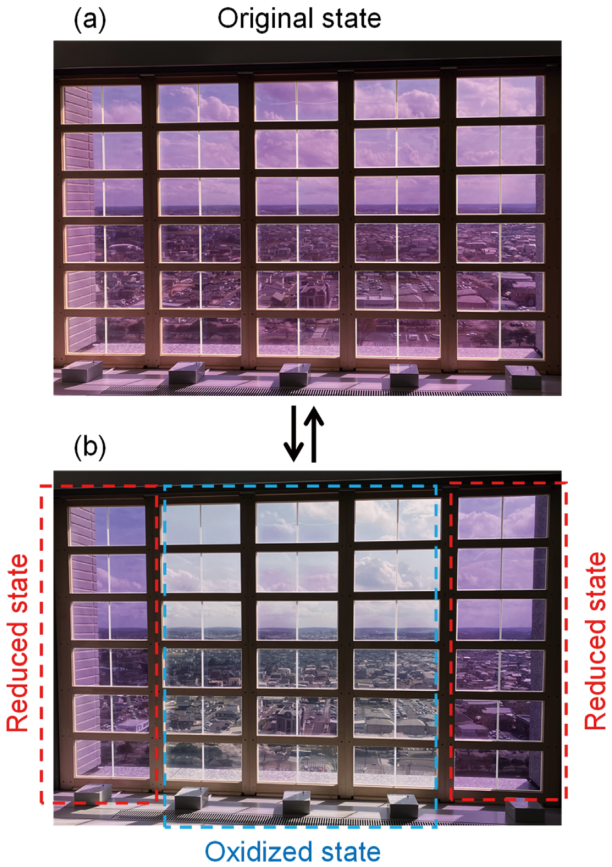

Fig. 4 EC smart window into a wooden framework (a) original state and (b) partially oxidized and reduced state of window after application of +1.5 and 0 V.

3.4 Evaluation of EC smart window performance

ECDs were installed into wooden frames for the application of smart windows in a south-facing window of a high-rise building in the Ibaraki Prefectural Government Office. The EC windows demonstrated clear, reversible EC transitions triggered by electrochemical redox reactions when subjected to applied potentials. As illustrated in Fig. 4, the original state of the EC smart window (Fig. 4a) exhibited a uniform purple coloration, due to the metal-to-ligand charge transfer occurring between Fe(II) center and the bis-terpyridine ligand moiety of MSP. Upon application of a potential of +1.5 V (Fig. 4b), a notable bleaching effect was observed due to the oxidation of Fe(II) to Fe(III), resulting in regions of smart window undergone EC transition from purple to a transparent, colorless state. Returning the voltage to 0 V reversed the oxidation, reinstating the reduced Fe(II) state and restoring the purple coloration. Visual inspections clearly depicted the EC switching capability of these windows, transitioning consistently between purple and colorless states upon the application of respective voltages. The operational stability and durability of the EC windows were rigorously evaluated under typical ambient environmental conditions, demonstrating reliable EC performance consistently throughout an extensive testing duration exceeding one year.

Regarding early operation, the deployed devices installed as smart window in the Ibaraki Prefecture building were switched at least once daily during the initial weeks following installation and were not subjected to continuous or high-frequency cycling. However, within the first month of operation, the bleached state could no longer be achieved at 1.5 V, necessitating the application of a higher voltage (3.0 V) to attain bleaching, which in turn led to a reduction in switching frequency to only a few times per month.

EC smart window utilizing was systematically evaluated for its EC performance, particularly focusing on color transition dynamics, uniformity, and stability over extended operational periods. For this evaluation, comparative analyses were conducted between a standard reference device (referred to as STD device) stored under controlled laboratory conditions more than 1 year and an operational device (referred to as the Ibaraki device) selected from among 60 devices deployed at the Ibaraki Prefecture building, after continuous real-

world usage within the same period. Movies capturing the EC transition processes were recorded for both devices, facilitating detailed analysis of the transition patterns at defined time intervals. Selected time-lapse images extracted from the movies (for the STD device and for the Ibaraki device) are presented in Fig. 5 and Fig. 6, respectively, showing the transition from purple (colored) to colorless (bleached) states.

Initially, the STD device exhibited a deep and saturated purple color (Fig. 5a) prior to voltage application, indicative of minimal exposure to environmental stresses. Time-lapse analyses at intervals of 2.00 s, 4.00 s, 8.00 s, 13.00 s, and 16.00 s, under an applied potential of 1.5 V, revealed gradual and complete bleaching at 16.00 s. We

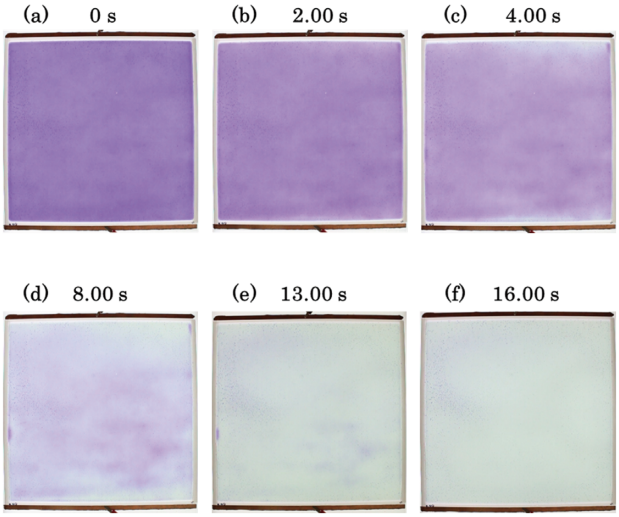

Fig. 5 Time-lapse images at (a) 0 s, (b) 2 s, (c) 4 s, (d) 8 s, (e) 13 s, and (f) 16 s of the STD device that was kept under laboratory conditions, showing EC transition at 1.5 V.

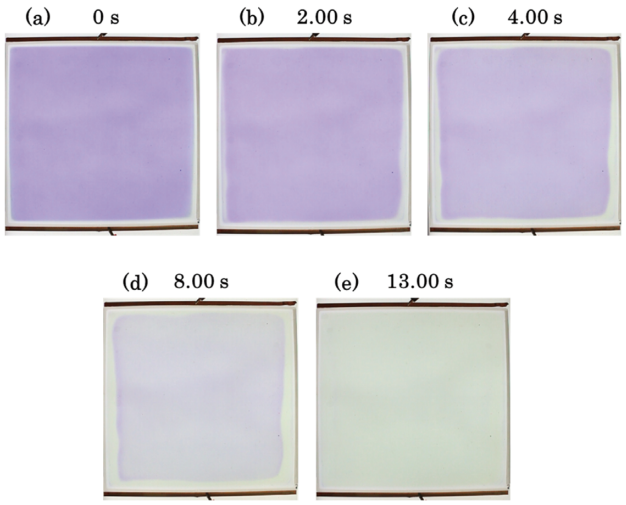

Fig. 6 Time-lapse images at (a) 0 s, (b) 2 s, (c) 4 s, (d) 8 s and (e) 13 s of the Ibaraki device that was used continuously as a smart window under real-world conditions, showing EC transition at 3.0 V.

investigated the EC properties of the STD at 3.0 V. The results were added in Fig. S1. The EC changes were almost same as those observed at 1.5 V. The device notably displayed subtle yet discernible non-uniformities, particularly around the edges. These non-uniformities likely arose due to localized micro-defects, potentially resulting from unnoticed physical or chemical degradation accumulated during long-term storage. Additionally, the relatively lower applied voltage of 1.5 V likely provided insufficient driving force to fully overcome localized resistance to ion transport or minor physical and chemical alterations, leading to incomplete and uneven bleaching in affected regions.

In comparison, the Ibaraki device, subjected to continuous real-world environmental exposure, displayed a visibly faded initial purple color (Fig. 6a). It is considered that this diminished color intensity is attributed primarily to environmental factors, such as daily sunlight exposure, fluctuating temperatures, and varying humidity levels. In addition, the device doesn't work at 1.5 V, probably because the counter material has been partially damaged. In our previous report,[26, 27] ECDs with a NiHCF counter electrode worked at 1.5 V, whereas devices without a counter material required voltages exceeding 2.5 V to attain the bleached state. Thus, in this work both the STD and Ibaraki devices were fabricated with the same NiHCF-based structure (Scheme S1) and initially worked at 1.5 V for bleaching. The Ibaraki device, however, stopped working at this voltage and required a higher driving potential (+3.0 V) to achieve a rapid and uniform EC transition. Furthermore, to confirm the degradation state of counter electrode films, the NiHCF layers from both the Ibaraki and STD devices were measured by optical microscopy (Fig. S2). However, no significant morphological differences were observed between the two electrodes, suggesting that nanoscale degradation may have occurred. Time-lapse images of Ibaraki device captured at 2.00 s (Fig. 6b), 4.00 s (Fig. 6c), 8.00 s (Fig. 6d), and 13.00 s (Fig. 6e) revealed uniform bleaching across the entire EC active area of 384.4 cm2, reaching a fully transparent colorless state within approximately 13.00 s at 3.0 V. This rapid and uniform transition, despite the reduced initial color saturation, demonstrated the robustness of the device's electrochemical processes (ion insertion/extraction) and confirmed that no irreversible degradation had occurred, even after one year of extensive real-world use.

To quantitative validation of these observations,

optical transmittance spectra were measured for both the STD and Ibaraki devices (Fig. S3 and Fig. 7). The optical properties were summarized in Table 3. The fading of the Ibaraki device was confirmed by the higher transmittance (T_c) in the colored state (12%) compared to the STD device (3%). The STD device exhibited an optical contrast (ΔT) of 57% at λ = 580 nm, while the Ibaraki device retained 66% despite its faded initial coloration. Both devices recovered their spectra after reduction, confirming that the faded color was fully reversible and not due to irreversible degradation. The STD device showed response times of t_b = 17.2 s (bleaching) and t_c = 12.2 s (coloration) at +1.5 to 0 V, whereas the Ibaraki device exhibited faster switching with t_b = 12.0 s and t_c = 5.6 s at +3.0 to 0 V.

These findings demonstrate that although prolonged environmental exposure may attenuate the initial coloration intensity of EC devices, their core electrochemical switching behavior and structural stability remain largely preserved. The results underscore the reversibility of the observed changes and highlight the critical role of optimizing driving voltage to maintain uniform switching performance under real-world operational conditions.

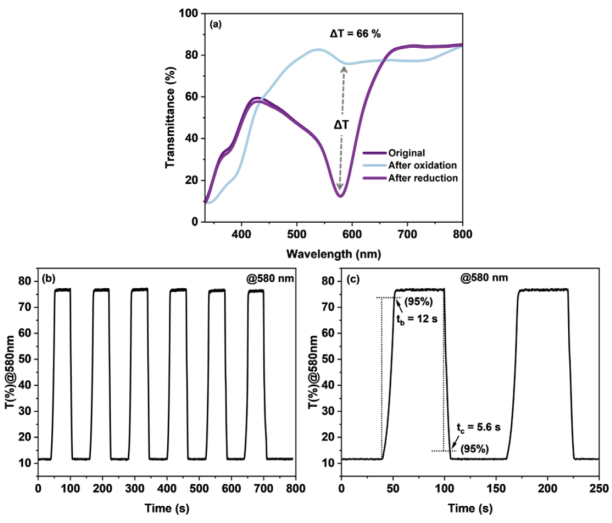

Fig. 7 (a) Transmittance spectrum of the Ibaraki device. The spectrum confirms a reversible color change with ΔT of 66% at 580 nm. (b, c) Time-resolved transmittance change at 580 nm during bleaching and coloration process, indicating a bleaching time (t_b) of 12.0 s and a coloration time (t_c) of 5.6 s based on 95% of ΔT.

Table 3 Optical properties of STD and Ibaraki devices.

Device	ΔT (%) at 580 nm	T_b (%)	T_c (%)	t_b (s)	t_c (s)	V_b (V)
STD	57	60	3	17.2	12.2	1.5
Ibaraki	66	78	12	12.0	5.6	3.0

4. Conclusion

In conclusion, we successfully fabricated and deployed a large-scale EC smart window utilizing polyFeL1, demonstrating its practical viability for energy-efficient building applications. The device exhibited rapid EC switching, with consistent coloration and bleaching behavior over extended operational use. After one year of real-world exposure in a south-facing window of a high-rise building, the EC window maintained its EC functionality, with only a slight reduction in initial color intensity and increase of the driving voltage due to environmental factors. Image-based analysis over time confirmed the uniformity of switching and a minimal degradation of performance over time. These analyses validate the structural and electrochemical stability of polyFeL1 as an effective material for smart windows. Future work will focus on optimizing polymer formulations and tailoring device architectures to preserve color depth, reduce switching voltages, and maintain long-term durability under diverse operational conditions.

Acknowledgement

This research work was financially supported by the Mirai project (grant number: JPMJMI21I4) from the Japan Science and Technology Agency (JST) and the Environment Research and Technology Development Fund (ERTDF) (JPMEERF20221M02) from Environmental Restoration and Conservation Agency (ERCA).

References

1) S.D. Rezaei, S. Shannigrahi, S. Ramakrishna: “A review of conventional, advanced and smart glazing technologies and materials for improving indoor environment”, Sol. Energy Mater. Sol. Cells, 159, 26-51 (2017)
2) M. Casini: “Smart Windows for Energy Efficiency of Buildings”, IJCSE, 2, 2372-3971 (2015)
3) Y.R. In, Y.M. Kim, Y. Lee, W.Y. Choi, S.H. Kim, S.W. Lee, H.C. Moon: “Ultra-Low Power Electrochromic Heat Shutters Through Tailoring Diffusion-Controlled Behaviors”, ACS Appl. Mater. Interfaces, 12 (27). 30635-30642 (2020)
4) H. Gundogdu, M. Terkes, A. Demirci, U. Cali: “Assessing energy savings and visual comfort with PDLC-based smart window in an Istanbul office building: A case study”, Energy Reports, 12, 4252-4265 (2024)
5) Z. Li, Z. Wu: “A study on the impact of electrochromic glazing on indoor environment”, J. Buil. Eng., 86, 108684 (2024)
6) S. Wu, H. Sun, M. Duan, H. Mao, Y. Wu, H. Zhao, B. Lin: “Applications of Thermochromic and Electrochromic Smart Windows: Materials to Buildings”, Cell. Rep. Phys. Sci., 4 (5), 101370 (2023)
7) X. Xie, H. Ji, L. Wang, S. Wang, Q. Chen, R. Luo: “Design and

Implementation of Electrochromic Smart Windows with Self-Driven Thermoelectric Power Generation", Nanomaterials, 14, 2079 (2024)
8) C.G. Granqvist, M.A. Arvizu, I. Bayrak Pehlivan, H.-Y. Qu, R.-T. Wen, G.A. Niklasson: "Electrochromic Materials and Devices for Energy Efficiency and Human Comfort in Buildings: A Critical Review", Electrochim. Acta, 259, 1170-1182 (2018)
9) S. Papaefthimiou, E. Syrrakou, P. Yianoulis: "Energy performance assessment of an electrochromic window", Thin Solid Films, 502, 257-264 (2006)
10) Q. Liu, Q. Chen, Q. Zhang, Y. Xiao, X. Zhong, G. Dong, M.-P. Delplancke-Ogletree, H. Terryn, K. Baert, F. Reniers, X. Diao: "In Situ Electrochromic Efficiency of a Nickel Oxide Thin Film: Origin of Electrochemical Process and Electrochromic Degradation", J. Mater. Chem. C, 6 (3), 646-653 (2018)
11) A.V. Shchegolkov, S.-H. Jang, A.V. Shchegolkov, Y.V. Rodionov, A.O. Sukhova, M.S. Lipkin: "A Brief Overview of Electrochromic Materials and Related Devices: A Nanostructured Materials Perspective", Nanomaterials, 11, 2376 (2021)
12) D. Dong, W. Wang, A. Rougier, A. Barnabé, G. Dong, F. Zhang, X. Diao: "Lithium Trapping as a Degradation Mechanism of the Electrochromic Properties of All-Solid-State WO3//NiO Devices", J. Mater. Chem. C, 6 (37), 9875-9889 (2018)
13) S. Macher, M. Rumpel, M. Schott, U. Posset, G.A. Giffin, P. Löbmann: "Avoiding Voltage-Induced Degradation in PET-ITO-Based Flexible Electrochromic Devices", ACS Appl. Mater. Interfaces, 12 (32), 36695-36705 (2020)
14) E.S. Lee, D.L. Dibartolomeo: "Application issues for large-area electrochromic windows in commercial buildings", Sol. Energy Mater. Sol. Cells, 1, 465-491 (2002)
15) C. Gu, A.-B. Jia, Y.-M. Zhang, S. X.-A. Zhang: "Emerging Electrochromic Materials and Devices for Future Display", Chem. Rev., 122 (18), 14679-14721 (2022)
16) V. Rai, R.S. Singh, D.J. Blackwood, D. Zhili: "A Review on Recent Advances in Electrochromic Devices: A Material Approach", Adv. Eng. Mater., 22, 2000082 (2020)
17) M. Higuchi: "Electrochromic Smart Materials: Fabrication and Applications", RSC, 13, 406-429 (2019)
18) M. Schott, H. Lorrmann, W. Szczerba, M. Beck, D.G. Kurth: "State-of-the-art electrochromic materials based on metallo-supramolecular polymers", Sol. Energy Mater. Sol. Cells, 126, 68-73 (2014)
19) M. Bera, C. Chakraborty, U. Rana, M. Higuchi: "Electrochromic Os(II)-Based Metallo-Supramolecular Polymers", Macromol. Rapid Commun., 39, 1800415 (2018)
20) M. Bera, Y. Ninomiya, M. Higuchi: "Stepwise introduction of three different transition metals in metallo-supramolecular polymer for quad-color electrochromism", Commun. Chem., 4, 56 (2021)
21) K. Fujii, D. Santra, M. Bera, T. Wakahara, R. Nagahata, M. Higuchi: "Electrochromic Ru-Based Metallo-Supramolecular Polymer with a Layered Inorganic–Organic Hybrid Nanocomposite for Improved Electrochemical Properties", ACS Appl. Polym. Mater., 5, 8808-8821 (2023)
22) C.-W. Hu, T. Sato, J. Zhang, S. Moriyama, M. Higuchi: "Three-Dimensional Fe(II)-based Metallo-Supramolecular Polymers with Electrochromic Properties of Quick Switching, Large Contrast and High Coloration Efficiency", ACS Appl. Mater. Interfaces, 6, 9118-9125 (2014)
23) S. Mondal, T. Yoshida, U. Rana, M. Bera, M. Higuchi: "Thermally stable electrochromic devices using Fe(II)-based metallo-supramolecular polymer", Sol. Energy Mater. Sol. Cells, 200, 110000 (2019)
24) A. Chernyshev, U. Acharya, J. Pfleger, O. Trhlíková, J. Zedník, J. Vohlidal: "Iron (II) Metallo-Supramolecular Polymers Based on Thieno[3, 2-b]thiophene for Electrochromic Applications", Polymers, 13, 362 (2021)
25) S. Mondal, T. Yoshida, M. Higuchi: "Electrochromic devices using Fe(II)-based metallo-supramolecular polymer: Introduction of ionic liquid as electrolyte to enhance the thermal stability", JSID, 27, 661-666 (2019)
26) H.-C. Lu, L.-Y. Hsiao, S.-Y. Kao, Y. Seino, D.C. Santra, K.-C. Ho, M. Higuchi: "Durable Electrochromic Devices Driven at 0.8 V by Complementary Chromic Combination of Metallo-Supramolecular Polymer and Prussian Blue Analogues for Smart Windows with Low-Energy Consumption", ACS Appl. Electron. Mater., 3 (5). 2123-2135 (2021)
27) M. Higuchi: "Stimuli-responsive metallo-supramolecular polymer films: design, synthesis and device fabrication", J. Mater. Chem. C, 2 (33). 9331-9341 (2014)

Shifa Sarkar received a bachelor's and master's degrees in chemistry from the Jagannath University, Dhaka, Bangladesh in 2019 and 2021. She is currently a doctoral student at the University of Osaka.

Kazuhiko Sakata obtained a master's degree in the Department of Synthetic Chemical Engineering at the Faculty of Engineering, Hokkaido University in 1982.

Yukio Fujii finished Graduate School of Engineering, Kyoto University in 1979 (MD, physical chemistry), worked for a chemical company until 2018. Technical staff in NIMS.

Masayoshi Higuchi obtained a PhD at the Graduate School of Engineering, Osaka University in 1998, worked at Keio University as Research Associate/Assistant Professor until 2004, then moved to National Institute for Materials Science (NIMS) as Senior Researcher. Since 2009, Group Leader. Since 2021, Guest Professor, the University of Osaka (concurrent). Studied on metallosupramolecular polymers and the electrochemical devices including electrochromic displays.